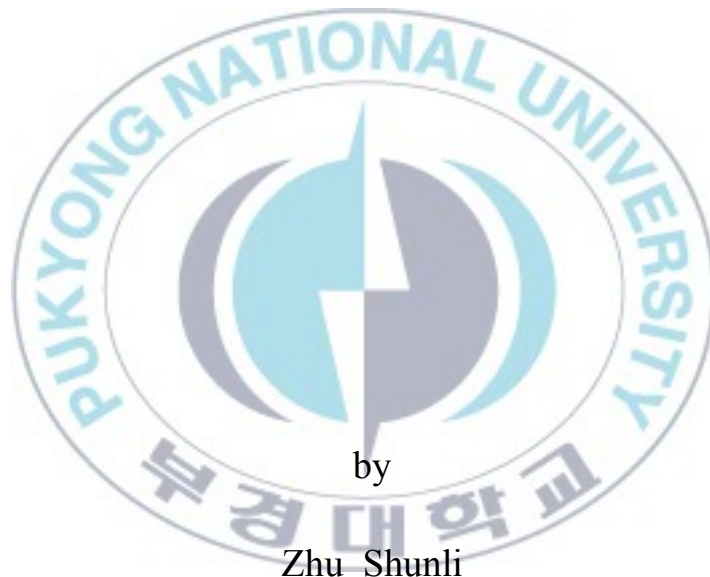


Thesis for the Degree of Master of Science

**A study of coastal upwelling with the
Passage of Typhoons in the East Sea**



by

Zhu Shunli

Department of Fisheries Physics
The Graduate School
Pukyong National University

August 2014

A study of coastal upwelling with the Passage of Typhoons in the East Sea

Advisor: Professor Chul-Hoon Hong



by

Zhu Shunli

A thesis submitted in partial fulfillment of the requirements
for the degree of

Master of Fisheries Science
Department of Fisheries Physics, The Graduate School,
Pukyong National University

August 2014

A study of coastal upwelling with the Passage of
Typhoons in the East Sea

A dissertation
by
Zhu Shunli

Approved by :

(Chairman)

(Member)

(Member)

(Member)

(Member)

August 2014

TABLES OF CONTENTS

Abstract	ii
1. Introduction	1
2. Numerical Model	2
3. Numerical results	5
3.1 Typhoon Oliwa Simulation	5
3.2 Numerical Experiments	10
3.2.1 Comparison of simulated typhoon in Case 1 and Oliwa	12
3.2.2 Dependence of Typhoon on pressure	13
3.2.3 Dependence of Typhoon on moving speed	13
3.2.4 Dependence of Typhoon on grid size	14
3.2.5 Dependence of Typhoon on track	15
4. Summary and Concluding Remarks	16
5. Acknowledgments	18
6. List of Figures	19
References	39

A study of coastal upwelling with the Passage of Typhoons in the East Sea

Zhu Shunli

Department of Fisheries Physics, The Graduate School,
Pukyong National University

Abstract

Coastal Upwelling is examined using a three-dimensional primitive equation model (POM) to simulate the observed-rapid SST decrease (Senjyu and Watanabe, 1999) along the northern Japanese coasts in the East/Japan Sea with the passage of Typhoon Oliwa (1997). The model successfully reproduces the observed SST decrease (-6 to -7 °C) including wind and atmospheric pressure, and reasonably explains it to be induced by coastal upwelling in a classical theory. In the model, we firstly demonstrate coastal upwelling with typhoon passage in the East Sea. The model shows that the upwelling weakly begins from earlier stage while Oliwa is located in low latitude, and fully develops (about 25 m/day) as Oliwa approaches the south of Kyushu, as well as being more excited in a narrow continental shelf of the northern Japanese coast. The model also suggests that the upwelling is affected by propagation of Kelvin waves along the Japanese coast. Case study gives more sophisticated information of coastal upwelling in this region by track, moving speed, and pressure of typhoons. The model suggests that upwelling was so predominant in the track of right-northward moving typhoon.

동해에서 태풍 통과 시 연안 용승의 연구

Zhu Shunli

부경대학교 대학원 수산물리학과

요약

연안용승이 3차원 원시모델(POM)을 이용하여 조사된다. 이 현상은 일본 북부 연안에서 태풍 올리와(Oliwa) 통과시 Senju 등(1999)이 관측한 해면수온의 급하강 현상의 모사를 통해 분석된다. 모델은 관측된 수온 및 기압을 포함 해수온도 하강(-6~-7°C)을 성공적으로 재현하며 고전적 이론에서 보여주듯 이들 현상이 연안용승에 의해 발생함을 잘 설명하였다. 모델은 우선 동해에서의 태풍통과시 연안용승을 잘 재현한다. 연안용승은 태풍 올리와가 저위도에 위치하는 이른 시기부터 약하게 발생하기 시작하다가 일본 규슈남쪽에 접근함에 따라 약 25m/일의 상승속도로 충분히 발전한다. 뿐만 아니라 용승은 일본 북부 연안에서 대륙붕이 매우 가파른 해역에서 보다 뚜렷이 발달하였다. 모델결과는 연안 용승이 일본연안을 따르는 켈빈파의 전파에 의해 영향을 받고 있음을 암시한다.

본 연구에서는 연안용승에 대한 케이스 연구(case study)를 통해 보다 유용한 정보를 얻을 수 있었다. 즉 태풍의 경로, 이동속도 및 중심기압 등의 변화에 따른 차이를 조사하였다. 그 결과 연안 용승은 정복으로 북상하여 규슈본토를 상륙하는 태풍의 경우 가장 뚜렷하게 발생했음을 보여주었다.

1. Introduction

The physical effects of hurricanes include deepening of the mixed layer and decreasing of the Sea Surface. A primary response to tropical cyclones (hereafter typhoons) is to cause upwelling. Many authors have reported this upwelling associated with physical and biogeochemical response. However, it seems that there have been a few reports of the SSC, especially in the coastal regions of the North Pacific, despite the fact that many typhoons very often land on the continents in this region. Senjyu and Watanabe (1999; hereafter SW) firstly observed a rapid SST decrease along the northern Japanese coast in the East/Japan Sea (here after the East Sea) with the passage of Typhoon Oliwa (1997) (Figure 1), and they implied that the SST decrease will be caused by coastal upwelling. With the passage of Typhoon Oliwa, five stations (Figure 1b) including Island Mishima recorded all the SST decrease ranging from 4 to 8°C (Figure 1c). A measurement in Island Mishima (dotted lines) was performed by a ferry boat before and after Oliwa. In fact, coastal upwelling can occur whenever the wind blows in parallel with a cost. The wind at Hamada (Figure 1d) was basically north-easterly along the northern Japanese coast when typhoon passes, thus most preferable here to coastal upwelling as pointed out by SW. In this study, we will examine how this rapid SST decrease using a three-dimensional numerical model. The goal of this paper is to address the mechanism how to cause the rapid SST decrease in the Northern Japanese coastal regions with the passage of

Typhoon Oliwa, and to elucidate dependence of upwelling on Typhoon's track, intensity, speed and grid size.

2. Numerical Model

The model (POM) used here, which was originally developed by Blumberg and Mellor (1987), is a three-dimension primitive equation model (3D model) same as Hong and Yoon (2003, hereafter HY) except for simulating Typhoon Oliwa instead of Typhoon Holly. The hydrostatic assumption and Boussinesq approximation are used. The model solves the following traditional hydrodynamics equations for conservation of mass, momentum, temperature, and salinity coupled with the equation of state,

$$\frac{\partial u}{\partial x} + \frac{\partial v}{\partial y} + \frac{\partial w}{\partial z} = 0, \quad (1)$$

$$\frac{\partial u}{\partial t} + u \frac{\partial u}{\partial x} + v \frac{\partial u}{\partial y} + w \frac{\partial u}{\partial z} - fv = -\frac{1}{\rho_0} \frac{\partial p}{\partial x} + \frac{\partial}{\partial z} \left\langle K_M \frac{\partial u}{\partial z} \right\rangle + F^x \quad (2)$$

$$\frac{\partial v}{\partial t} + u \frac{\partial v}{\partial x} + v \frac{\partial v}{\partial y} + w \frac{\partial v}{\partial z} + fu = -\frac{1}{\rho_0} \frac{\partial p}{\partial y} + \frac{\partial}{\partial z} \left\langle K_M \frac{\partial v}{\partial z} \right\rangle + F^y \quad (3)$$

$$\rho g = -\frac{\partial p}{\partial z} \quad (4)$$

$$\frac{\partial T}{\partial t} + u \frac{\partial T}{\partial x} + v \frac{\partial T}{\partial y} + w \frac{\partial T}{\partial z} = \frac{\partial}{\partial z} \left\langle K_H \frac{\partial T}{\partial z} \right\rangle + F^T \quad (5)$$

$$\frac{\partial S}{\partial t} + u \frac{\partial S}{\partial x} + v \frac{\partial S}{\partial y} + w \frac{\partial S}{\partial z} = \frac{\partial}{\partial z} \left\langle K_H \frac{\partial S}{\partial z} \right\rangle + F^S \quad (6)$$

$$\rho = \rho(T, S) \quad (7)$$

Where x, y are coordinates along the longitude and latitude, respectively. K_H is the vertical eddy diffusivity, K_M is the vertical eddy viscosity, $F^{(X,Y)}$ the horizontal eddy friction terms, and $F(T,S)$ the horizontal eddy diffusion terms. Knudsen's equation is utilized to solve equation (7). The K_M and K_H are calculated using the Mellor and Yamada level 2.5 turbulence closure model [Galpern et al., 1988]. f is the Coriolis force.

Briefly repeating the salient points of *HY*, the model is formulated by a Cartesian coordinate with bottom-following, sigma-coordinate system. In the initial conditions, vertical temperature is linearly given from 27 °C at the surface, and salinity is assumed to be equal everywhere to 34.5 psu to consider here thermodynamics only. At open boundaries (dashed line in Figure 1), the internal normal velocity is governed by a Sommerfeld radiation condition; an elevation is specified as the external open boundary condition; a slippery condition is employed for temperature. For simplicity, no air-sea heat exchange and no basic currents, such as the Kuroshio and Tsushima Current, are considered. The bottom topography from

the NOAA National Data Center has a maximum depth of 3600m (Figure 2, top) has been smoothed so that the sigma coordinate system does not cause spurious current in the region of steep topographic gradients. The model domain is bounded by 24°30'N-52°00'N and 117°25'E-143°00'E including a whole area of the East China Sea, the Yellow Sea, and the East sea. An extended map around the Korean/Tsushima Straits is shown as Figure 2 (bottom) to investigate seawater variations with coastal upwelling more in detail. The model results obtained from each station (A~D in Figure 2, bottom) which corresponds to KJ, KY, HA, and Island Mishima, respectively, will be compared with the observed SST.

The number of vertical sigma levels is 26, being finer in the upper ocean. Horizontal resolutions are 20 km in both x and y directions, which are substantially enough to resolve an internal Rossby radius (about 50~60 km) in an upwelling region (~100m; 35 °N). In atmospheric conditions of the model, we use very simple-conventional equations; the air pressures and the winds are given Fujita's equation (1952) and Miyazaki et al. (1961), respectively. This underlies that the goal of this paper is to qualitatively understand physical process causing the coastal upwelling so that we do not require a real typhoon in the model. Refer to *HY* for a complete description of the model. Typhoon Oliwa (see Figure 1 for its track) occurred at 00:00 (local time) September 4th, 1997 (hereafter 04:0000), landed at 16:0900 on Kyushu, and ended its life at 17:2100 when it was changed to a weak cyclone. The model runs for 15 days from 07:2100 (18°42'N-152°18'E) to 22:2000, and involves most of life times

of Oliwa.

3. Numerical results

3.1 Typhoon Oliwa Simulation

We begin to show the time series of the SST simulation (Figure 3) in the model. The model successfully reproduces the observed SST decrease at each station (Figure 2, bottom) in aspects of tendency to rapidly decrease the SST, the time to reach the SST minimum (late September 16) and the cooling amplitudes (4-7°C). However, the model has slightly higher value (~25°C) of the SST minimum at Is Mishima than that in the observation (~22°C), and showed a tendency to rapidly increase a few degrees of the SST at each station after the typhoon dead (about 17:0000). This will be discussed later, concerning with limitations of the model. On the other hand, in the model, the wind (Figure 3c) and the air pressure (Figure 3d) at St. C also well corresponds to the observation (HA, Figure 1d) in aspects of variation patterns in time and roughly their amplitudes, e.g., the maximum wind (~18 m/sec), although the lowest air pressure (~994 hpa) is more intensified than that at HA (~998 hpa).

In a classical theory of coastal upwelling (e.g., Yoshida, 1955), it has been known that coastal Jet frequently occurs as resulted from geostrophic equilibrium that is established by

balancing the pressure gradient force with the Coriolis force. Time series of velocity at St. C (HA) (Figure 3d) shows that south-westward flow is weakly formed from earlier time when Oliwa was located in low latitude and is fully developed (~ 1 m/sec) with the passage of Oliwa. Sea surface elevation (Figure 3e) here well reflects this flow field from the earlier time, i.e., negative sea level is caused by Ekman transport (presented later in Figure 5) due to the north-easterly wind (Figure 3b), resulting in inducing the Jet, and reaches the maximum (~ 30 cm) half a day after Oliwa's passage. On 15th August, however, the elevation temporarily shows positive sea levels for a day. This is caused by propagation of Kelvin waves along the Japanese coast (Figure 4). From earlier time Kelvin waves is created propagates at 13:0900 and weakly propagates along the northern Japanese coast (Figure 4a), as negative amplitude Kelvin waves. As Oliwa approaches the south Kyushu (Figure 4b-4c), the Kelvin waves fully develops and propagates (Figure 4b-4d) as positive amplitude Kelvin waves, i.e., the positive amplitude Kelvin waves consecutively propagates from the southern Japanese coast in the North Pacific to the northern Japanese coast in the East Sea, as earlier pointed out by some authors (e.g., HY). After the propagation of the positive amplitude Kelvin waves, the elevation (Figure 3e) becomes negative again due to strong alongshore wind (Figure 3b), and reaches the minimum earlier on

Sept. 17, showing the SST minimum (Figure 3a), when Oliwa passes around St. C. In this period, it should be noted that cooled water regions ($\sim 26^{\circ}\text{C}$) are extensively spread to the Yellow Sea and the East Sea (Figs. 4b-4d) from the central region of the typhoon.

Next consider the coastal upwelling in vertical velocity fields (Figure 5). Time evolutions of vertical velocity field on Section A (see Figure 2, bottom) show that vertical velocity field (coastal upwelling) fully develops during 16:0900 (Figure 5b)-16:2100 (Figure 5c) when Typhoon Oliwa provides the most preferable wind (the north-easterly wind) to coastal upwelling along the Japanese coast in the East Sea (Figure 3b), i.e., this period coincides with time when the typhoon is in the closest proximity of St. C (HA). Thus, the model clearly shows that the observed SST cooling by SW was induced by coastal upwelling. In the model, the upwelling velocity has been estimated by 18-35 m/day. Considering the depths (50-100m) around the coastal regions, this speed is enough to raise bottom water to the surface for several days while Oliwa passes, and may be comparable to values in the previous studies, e.g., the order of 1-2 m day⁻¹ usually and sometimes possibly 10 m day⁻¹ (Colling, 1982?). On the other hand, when the typhoon track roughly orientates to the north from Sept. 14 to 16, the SST rapidly decreased (Figs. 1a and 1c), and the model also well identified this affairs (Figure 3a),

associated with preferable wind to coastal upwelling. This implies that the coastal upwelling in this region may be seriously dependant on typhoon's tracks.

In the initial condition, the model domain is bounded by $24^{\circ}30'N$, $52^{\circ}00'E$ and $117^{\circ}25'N$, $143^{\circ}00'E$. The model results obtained from each station(A~D in Figure 2,bottom) which corresponding to KJ,KY,HA, and Island Mishima, respectively, will be compared with the observed SST .In early times (Figure 4a-b), Typhoon Oliwa moved westward, developing into a strong typhoon with the lowest central pressure of 915 hpa (10:1800) (see Figure 1a). At 15:0000, Typhoon Oliwa is located northeast of Taiwan (Figure 4c) after moving into the continental shelf in the East China Sea. The central area shows the higher sea level due to isostatic effect (inverse barometer effect) and the SST cools in the rear of the typhoon. Then, typhoon moved northeastward, passing through the Korea Strait and upwelling occurs in the rear of typhoon. In the model, we simulate the time series of the SST and the SST decrease at each station is produced at each station (Figure 3a) in terms of the tendency to rapidly decrease the SST, the time to reach the SST minimum and the cooling amplitudes .On the other hand,in the model, the wind (Figure 3b) and the air pressure (Figure 3c) at St.C (Hamada) also well simulate the observation (HA. Figure1d) with respect to variation patterns in time and roughly their

amplitude. For instance, the maximum wind (~ 18 m/sec), although the lowest air pressure (~ 994 hpa) is more intensified than that at HA (~ 998 hpa).

Time series of velocity at St. C (HA) (Figure 3d) shows that the south-westward flow is weakly formed from an earlier time when Oliwa was located in low latitude and is fully developed (~ 1 m/sec) with the passage of Oliwa. Sea surface elevation (Figure 3e) here well reflects this flow field from the earlier time, i.e., n

The negative sea level is caused by Ekman transport (presented later in Figure 5) due to the north-easterly wind (Figure 3b), and reaches the maximum (~ 30 cm) half a day after Oliwa's passage. On 15th August, however, the elevation temporarily shows positive sea levels for a day. This is caused by propagation of Kelvin waves along the Japanese coast (Figure 4). From earlier times Kelvin waves propagate at 13:0900 and weakly propagates along the northern Japanese coast (Figure 4a), as negative amplitude Kelvin waves. As Oliwa approaches the south Kyushu (Figure 4b-4c), the Kelvin waves fully develops and propagates (Figure 4b-4d) as positive amplitude Kelvin waves, i.e., the positive amplitude Kelvin waves consecutively propagates from the southern Japanese coast in the North Pacific to the northern Japanese coast in the East Sea, as earlier pointed out by some authors . After the propagation of the positive

amplitude Kelvin waves, the elevation (Figure 3e) becomes negative again due to strong alongshore wind (Figure 3b), and reaches the minimum earlier on Sept. 17, showing the SST minimum (Figure 3a), when Oliwa passes around St. C. In this period, it should be pointed out that cooled water regions ($\sim 26^{\circ}\text{C}$) are extensively spread to the Yellow Sea and the East Sea (Figure 4b-4d) from the central region of the typhoon.

Next consider the coastal upwelling in vertical velocity fields (Figure 5). Time evolutions of vertical velocity field on Section A (see Figure 2, bottom) show that vertical velocity field (coastal upwelling) fully develops during 16:0900 (Figure 5b)-16:2100 (Figure 5c) when Typhoon Oliwa provides the most preferable wind (the north-easterly wind) to coastal upwelling along the Japanese coast in the East Sea (Figure 3b). Thus, the model is a clear identification that the observed SST cooling by SW was induced by coastal upwelling. Nevertheless, in the coastal region, sea surface cooling continues for several days.

3.2 Numerical Experiments

It has been known that upwelling caused by typhoon can result in sea surface temperature drop along the typhoon track. The ocean response to Typhoon has been investigated through observation methods or numerical methods (e.g. M.García-Reyes

and J.Largier,2010; Dongxiao Wang et al et al., 2012; Shoude Guan et al.,2014;). However, few scientists use POM as the effective model to study the coastal upwelling in the East/Japan Sea. Case studies are to focus on the dependence of tracks, moving speed, pressure and grid interval. The model is same as Oliwa simulation except for domain area and different track of Typhoon (Figure 6). The model has a horizontal resolution of 20km in both x and y directions from its from its left-southern-most grid point ($20^{\circ}\text{N},117^{\circ}\text{E}$) to its right-northern-most grid point ($52^{\circ}\text{N},144^{\circ}\text{E}$), including a whole area of East China Sea, the Yellow sea, the East Sea and Taiwan. The left-hand side (LHS) track starts from the grid point ($13^{\circ}43'\text{N},130^{\circ}43'\text{E}$) to the grid point ($39^{\circ}59'\text{N},120^{\circ}16'\text{E}$), the central track (CTR) begins from grid point ($13^{\circ}43'\text{N},130^{\circ}43'\text{E}$) to grid point ($38^{\circ}15'\text{N},130^{\circ}42'\text{E}$), and the right-hand side track starts from grid point ($13^{\circ}43'\text{N},130^{\circ}43'\text{E}$) to the grid point ($40^{\circ}6'\text{N},141^{\circ}07'\text{E}$) (Figure 7 upper). Numerical experiments, which target is to understand upwelling during and subsequent to the passage of Typhoon is performed using POM model. Detailed objectives of the numerical simulation are the following:

1. To compare simulated typhoon in case 1 and Oliwa.
2. To investigate the Dependence of typhoon on pressure .
3. To investigate the Dependence of typhoon on on moving speed.
4. To investigate the Dependence of typhoon on on grid.

5. To investigate the Dependence of typhoon on on track.

3.2.1 Comparison of simulated typhoon in Case 1 and Oliwa

Figure 11 represents the time series of the SSTs at four stations(Case 1 in table 1). One can say that the SSTs drop at each station is produced from a slightly earlier time (Figure 8) compared with Oliwa (Figure 3a). As the Simulated Typhoon approaches the St.C (Figure 11a), the negative sea elevation (Figure 9d) and positive vertical velocity (Figure 10) are caused by upwelling due to east wind (Figure 9a). After the Typhoon passes from the South of Japan (Figure 11b) to the East Sea(Figure 11c), the positive sea elevation (Figure 9d) and negative vertical velocity (Figure 10) are caused by downwelling due to west wind (Figure 9a). SST decrease continues and then oscillates for the remaining of the time (Figure 10). Thus, this result shows that before the passage of the typhoon SST at St.C decrease is mainly led with upwelling. The vertical velocity at 50m is larger than that at 25m, 50m depth (Figure 10). That is, the upwelling is stronger at 50m depth than at sea surface. The wind (Figure 9a) , air pressure (Figure 9b), flow velocity (Figure 9c), and elevation (Figure 9d) at St.C (Hamada) are similar to the results in the Oliwa Simulation (Figure 3) with respect to variation patterns in time and roughly their amplitude.

3.2.2 Dependence of Typhoon on pressure

To qualify the impact of upwelling on hurricane intensity, figure 12 shows simulated SSTs of all physical parameterizations (Case 1, 2, 3 in table 1) on pressure: 950 hpa (Figure 12a), 970 hpa (Figure 12b), 990 hpa (Figure 12c). The model at high pressure has slightly higher value of the SST minimum at Is Mishima than that at lower pressure. The SST decreases gradually from initial time and starts to show sudden decrease from 150 hours when the typhoon is located at 238 km south of Kyushu. As typhoon approaches (Vertical line in figure 12a) Station C, the SST at 950 hpa decreases 16°C rapidly and then increases 11°C, while the SST at 970 hpa decreases 14°C (Figure 12b), and the SST at 990 hpa decreases 6°C (Figure 12c). The decrease of the SST appears to be irreversible and is caused by upwelling. In other way, one can say that the lower the central pressure, the stronger the upwelling in the northern Japanese coast.

3.2.3 Dependence of Typhoon on moving speed

To qualify the impact of upwelling on moving speed, figure 13 represents simulated SSTs of all physical parameterizations

(Case 1, 4, 5 in table 1) on moving speed: 3 m/s (Figure 13a), 6 m/s (Figure 13b), 9 m/s (Figure 13c). One can see that the SST differences at four stations are small during the first 150 hours; The SST simulation at 3 m/s decreases 14°C during the passage of Typhoon (vertical line in figure 13a), which is larger than 9°C decrease of simulation at 6 m/s, and 6°C decrease of simulation at 9 m/s respectively. After Typhoon passes, the SST at 3 m/s increases 6° rapidly, and then grows slowly. While the SSTs at 6 m/s and 9 m/s gradually grows, which are caused by weak typhoon effects. Thus, the faster the moving speed, the less cool the sea water. It means that upwelling becomes weaker as the moving speed of typhoon is faster.

3.2.4 Dependence of Typhoon on grid size

To qualify the impact of upwelling on moving speed, figure 14 shows simulated SSTs of all physical parameterizations (Case 1, 6 in table 1) on grid size: 10 km (Figure 14a) and 20 km (Figure 14b). The other physical parameterizations as follows: moving speed is 3 m/s at central track and central pressure is 970 hpa. The model shows similar SST variations on different grid size. At 10 km grid interval, The SST at St.C decrease 13.5 °C when typhoon passes over (vertical line in Figure 14a); while The SST of 20 km grid interval at St.C decrease 14 °C as typhoon passes over (vertical line in Figure 14b). It was true that SST

decrease does not depend on the grid interval (Figure 14c). As a result, the SST variations are not largely different from each other, that is, grid sizes in the model do not influence upwelling state significantly.

3.2.5 Dependence of Typhoon on track

To qualify the impact of upwelling on track, figure 15 shows simulated SST of all physical parameterizations (Case 1, 7, 8 in table 1) on track: left-hand side track (Figure 15a), central track (Figure 15b) and right-hand side track (Figure 15c). In the LHS and RHS track (Figure 6), SST cooling is small ($1.5\text{-}2^{\circ}\text{C}$) which is caused by weak effect of Typhoon. The SST of the central Track at St.C decrease 14°C as typhoon over (vertical line in figure 15b) and increase 4°C (Figure 15b). There was an irregular oscillation of 0.5°C amplitude after the storm passage. The SST then stabilized and remained approximately for the remainder of the time. On the left-hand and right-hand of track, the Typhoon SST at St.C decrease 1.5°C (Figure 15a, c) during the whole simulation time.

It was summarized that in the cases of RHS and LHS (Figure 15a, c), except for the CTR track, the SST has almost no influences. Consequently, in the model, coast upwelling in the northern Japanese coast was most predominant in the CTR (central) track of the typhoon, in which the typhoon moves right-

northward.

4. Summary and Concluding Remarks

In this paper a three-dimensional primitive equation model (POM) was implemented to examine the observed SST decrease (*Senjyu and Watanabe, 1999*) in the northern Japanese coast in the East Sea during Typhoon Oliwa. The model successfully well reproduced the observed-prominent features, such as a SST decreasing tendency in time and space, and sufficiently described how they happened. The model concludes that the SST decrease has been caused by coastal upwelling to complement Ekman transport, especially while Oliwa provides a preferable wind to coastal upwelling evolution, i.e., the north-easterly wind parallel to the coast.

Since a basic theory about coastal upwelling was first presented by *Yoshida (1955)*, many studies for the upwelling have been carried out (e.g. *Suginohara, 1974; Gill, 1982; Cushman-Roisin, 1994*). In the model, there have also been a few studies with the passage of typhoons, probably because of mainly using 2D models (e.g., *Platzman, 1963; Unoki et al., 1964; Konishi and Tsuji, 1995*). In the present study, the model realistically provides illustrations of coastal upwelling in the East Sea with typhoon's passage, and strongly suggests that typhoons may induce anywhere coastal upwelling (or sinking) along the coasts in the north Pacific although there have not been a few observations yet. *Lee et al. (200?)* reported that homogenous

coastal water ($\sim 27^{\circ}\text{C}$) in the vertical (about 30m depth) was observed in the southern sea of Korean peninsula after Typhoon Maemi (2003) in the super class. This may be partly addressed by coastal downwelling (vertical mixing) excited due to wind paralleled with the southern coast of Korea.

SW showed that the most SST cooling was observed at Hamada ($\sim -8^{\circ}\text{C}$) (Figure 1c), and the model well reproduced such SST cooling at St. C (Figure 3a), corresponding to Hamada. According to Oke and Middleton (2000), this may be a sharp continental shelf in this region (Figure 1b; Figure 2, bottom), i.e., they reported that upwelling induced by topography develops over a narrow continental shelf because of establishing a high bottom stress region. However, this effect of a shelf should be studied more in precise horizontal resolutions because the grid size (20 km) in the model may not be enough to resolve the shelf around the northern Japanese coast.

The model was simplified to capture basic key points. For example, air-sea heat interaction has been excluded, and thus the model results may modify SSC, especially toward weakening it as discussed by *Sakaida et al.* (1998). Basic currents, such as the Kuroshio and the Tsushima Current, were also negligible. Since the Kuroshio will cross a track of Typhoon Oliwa, in particular, the model results may be influenced in momentum flux, and the Tsushima Current may also affect coastal upwelling evolution in the northern Japanese coastal region of the East Sea. In order to simulate typhoons in reality, these points should be complemented. Nevertheless, physical concepts in the model will not be significantly contaminated by these assumptions.

The model well reproduced the rapid SST decrease observed in the northern Japanese coast with the passage of Typhoon Oliwa and clarified that this is caused by coastal upwelling. Upwelling is the primary mechanism that lowers the SST beneath a moving hurricane, causing a significant enhancement of the SST response. The coastal upwelling is largely depended on tracks, intensity, and moving speed of typhoon.



5. Acknowledgments

I would like to thank the committee members of the fisheries department for their time and helpful comments regarding the contents of this study. Special thanks to my major professor Dr. Chul-Hoon Hong for his suggestion and patience during my research.

6. List of Figures

Figure 1. (a) A track of Typhoon Oliwa. Left and right numerals on the track represent atmospheric pressures and dates at every 09:00 o'clock, and the dotted line denotes open boundaries in the model. (b) The observed stations in the northern Japanese coast. (c) Time series of SST at each station; dotted plot represents the observation by a ferry boat at Is. Mishima before and after the typhoon passage; temperature values in the ordinate axis are adjusted for visual convenience. (d) Wind at Hamada (HA) in this period. (b) (c), (d) are reproduced from SW.

Figure 2. Model bathymetry (top) (depth in meters). The contour interval is 300m except for 20m in the Yellow Sea and the East China Sea. An enlarged region around the Korean Strait (bottom) is given, and transect A (bottom) gives cross sectional profiles of velocity and temperature in the East Sea. Stations A, B, C, and D correspond to KJ, KY, HA, and Is Mishima in SW's observation (Figure 1b), respectively.

Figure 3. (a) Time series of SST at Stations A~D (Figure 2, bottom), corresponding to KJ, KY, HA, and Is Mishima (Figure 1b). The values are given in the first level of the model. At St. C (corresponding to HA), calculated (b) wind (m/sec), (c) atmospheric pressure (hpa), (d) velocity (cm/sec), and (e) sea surface elevation (cm) are given. Vertical bar in Figs. 3b-3e

represents a time when Oliwa passed in close proximity of St. C.

Figure 4. Time evolutions (13:0900-16:0900) (Figure 5a-5d) of sea water variation in elevation (contours), SST (colors), and velocity (arrows) one day apart. Velocities less than 10cm/sec are eliminated for visual convenience. C.I. =5cm.

Figure 5. Time evolutions (15:2100-19:0900) of coastal upwelling ((a)-(d)) on Section A (see Figure 2, lower) every 12 hours. Note that vertical velocity ($\times 10^{-3}$ cm/sec) is exaggerated for visual convenience.

Table 1. Conditions of each experiment in the case study.

Figure 6. Three tracks of Typhoon in the simulation at every 12 hour . LHS represents left-hand side of track starts from the grid point ($13^{\circ}43'N, 130^{\circ}43'E$) to the grid point ($39^{\circ}59'N, 120^{\circ}16'E$), CTR represents the central track starts from the grid point ($13^{\circ}43'N, 130^{\circ}43'E$) to the grid point ($38^{\circ}15'N, 130^{\circ}42'E$) and RHS represents the Right-hand side of the track starts from grid point ($13^{\circ}43'N, 130^{\circ}43'E$) to the grid point ($40^{\circ}06'N, 141^{\circ}07'E$).

Figure 7. A new Model bathymetry (top) (depth in meters). The contour interval is 300m except for 20m in the Yellow Sea and the East China Sea. An enlarged region around the Korean Strait (bottom) is given, and transect A (bottom) gives cross sectional profiles of velocity and temperature in the East Sea. Stations A, B, C, and D correspond to KJ, KY, HA, and Is Mishima in SW's observation (Figure 1b), respectively.

Figure 8. Time series of SST of Typhoon at a moving speed of 3 m/s with the central pressure 970 hpa at Stations A~D (Figure 7, bottom), corresponding to KJ, KY, HA, and Is Mishima (Figure 1b). Vertical bar in Figs. 3b-3e represents a time when Typhoon passed in close proximity of St. C.

Figure 9.(a) Time series of (a) wind (m/s), (b) atmospheric pressure (hpa), (c) velocity (cm/sec), and (d) sea surface elevation (cm) are given. Vertical bar in Figs. 3a-3d represents a time when Typhoon passed in close proximity of St. C.

Figure 10. Time evolutions of vertical velocity and temperature values at a depth of 16m, 25m, and 50m respectively at Stations C (Figure 7, bottom), Vertical bar represents a time when Typhoon passed in close proximity of St. C.

Figure 11. Time evolutions (168-240 hours) (Figure 5a-5d) of sea water variation in elevation (contours), SST (colors), and velocity (arrows) . Velocities less than 10cm/sec are eliminated for visual convenience. C.I. =5cm.

Figure 12. Time series of SST of Typhoon moving along the central track at a constant moving speed of 3m/s at Stations A~D (Figure 7, bottom) , corresponding to KJ, KY, HA, and Is Mishima (Figure 1b) on condition of different minimum central pressure (950hpa(a), 970hpa(b), 990hpa(c)). Comparison of SST in the same coordinate system is showed (d). Vertical bar

represents a time when Typhoon passed in close proximity of St. C.

Figure 13. Time series of SST of Typhoon moving along the central track with the minimum central pressure 970 hpa at Stations A~D (Figure 7, bottom) , corresponding to KJ, KY, HA, and Is Mishima (Figure 1b) on condition of different moving speed (3m/s(a), 6m/s(b), 9m/s(c)). Vertical bar represents a time when Typhoon passed in close proximity of St. C.

Figure 14. Time series of SST of Typhoon moving along the central track at a constant moving speed of 3m/s with the same minimum central pressure 970 hpa at Stations A~D (Figure 7, bottom) , corresponding to KJ, KY, HA, and Is Mishima (Figure 1b) on condition of different grid interval(10 km(a), 20 km(b)). Comparison of SST in the same coordinate system is showed (c). Vertical bar represents a time when Typhoon passed in close proximity of St. C.

Figure 15. Time series of SST of Typhoon at a moving speed of 3 m/s with the central pressure 970 hpa at Stations A~D (Figure 7, bottom) , corresponding to KJ, KY, HA, and Is Mishima (Figure 1b) on condition of different moving track(LHS(a), CTR(b),RHS(c)). Comparison of SST in the same coordinate system is showed (d). Vertical bar represents a time when Typhoon passed in close proximity of St. C.

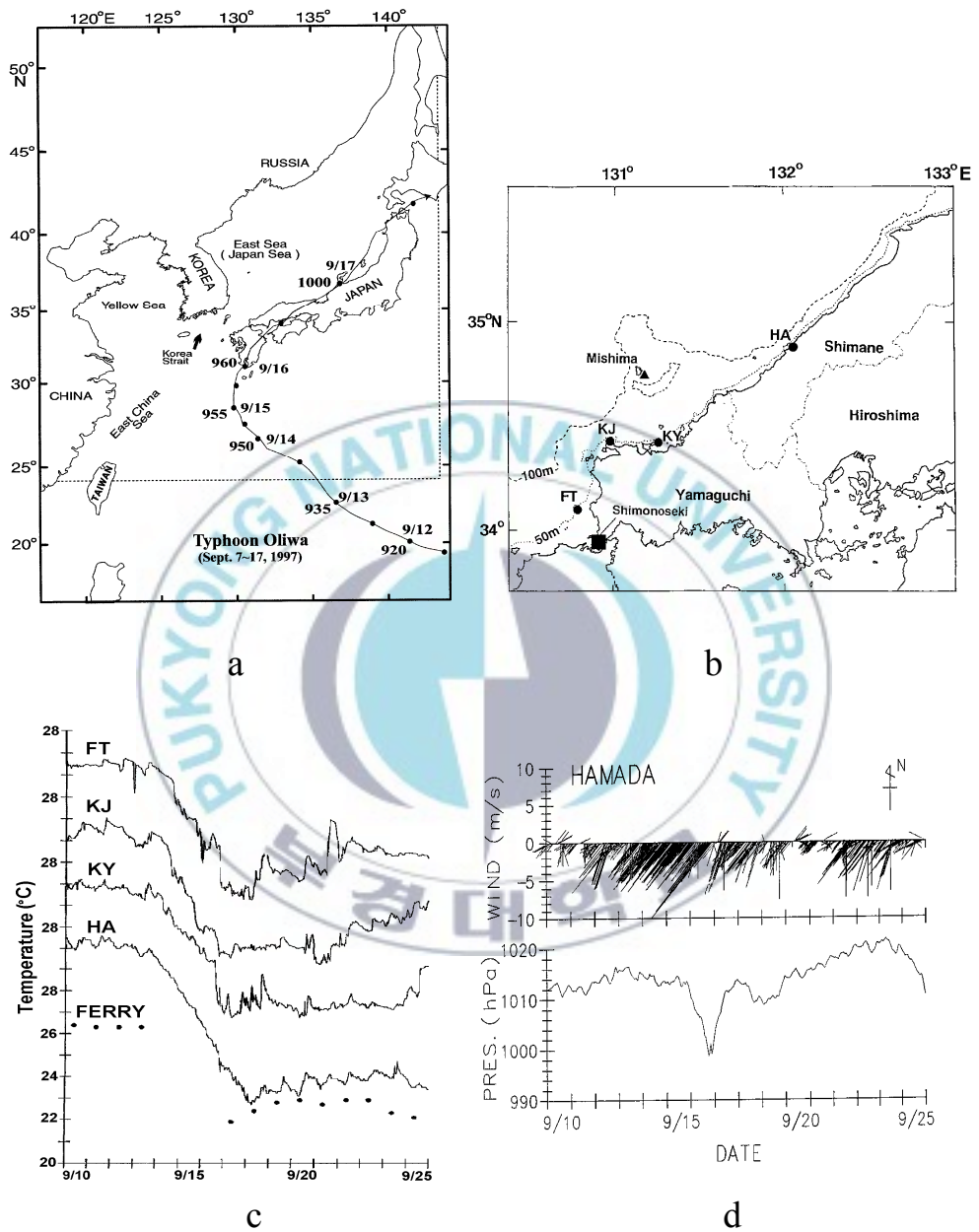


Figure 1

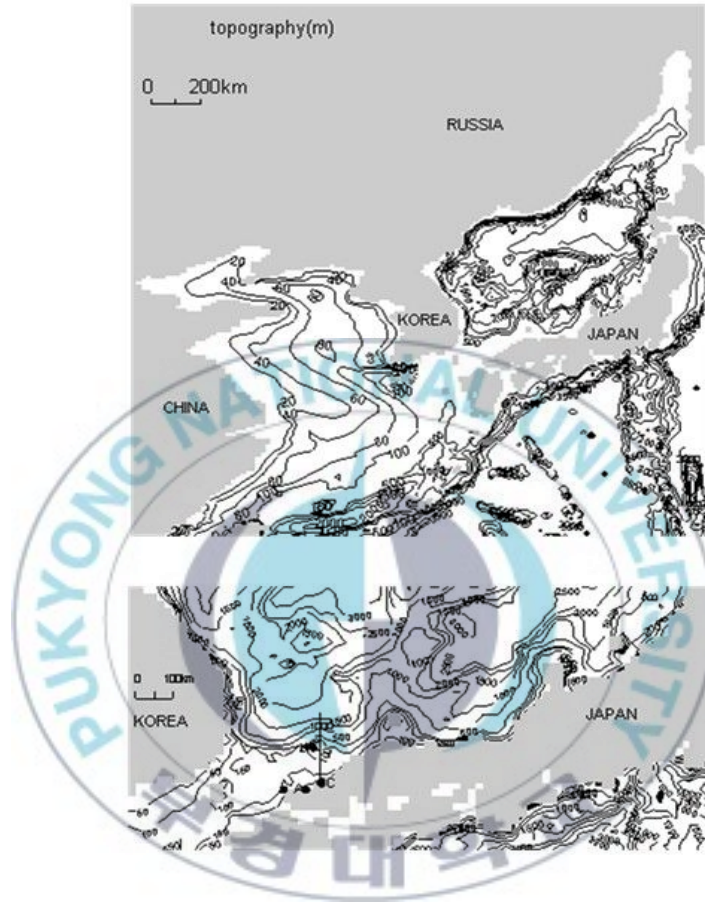


Figure 2

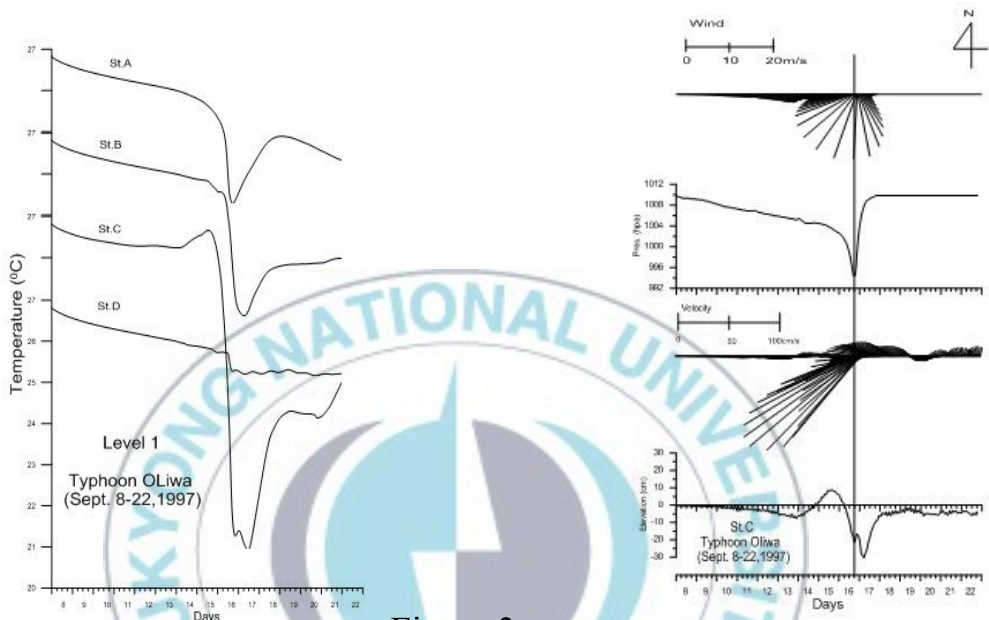


Figure 3

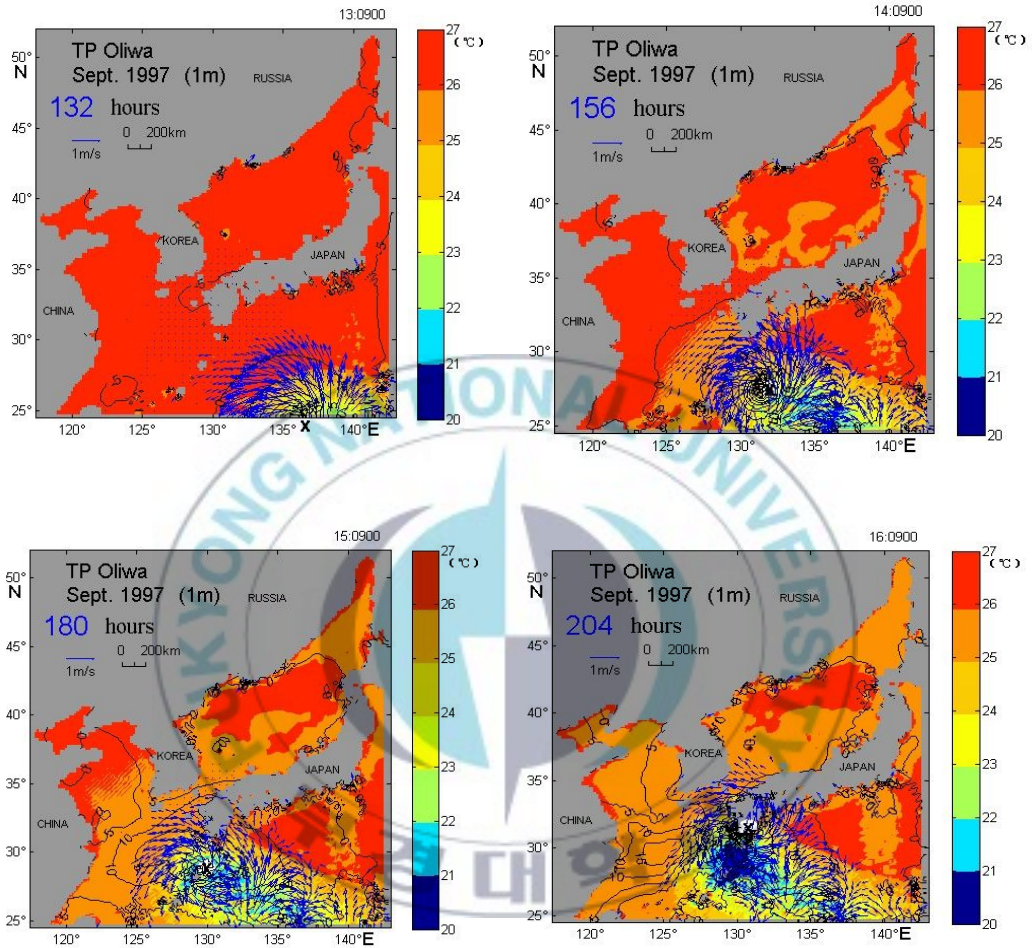


Figure 4

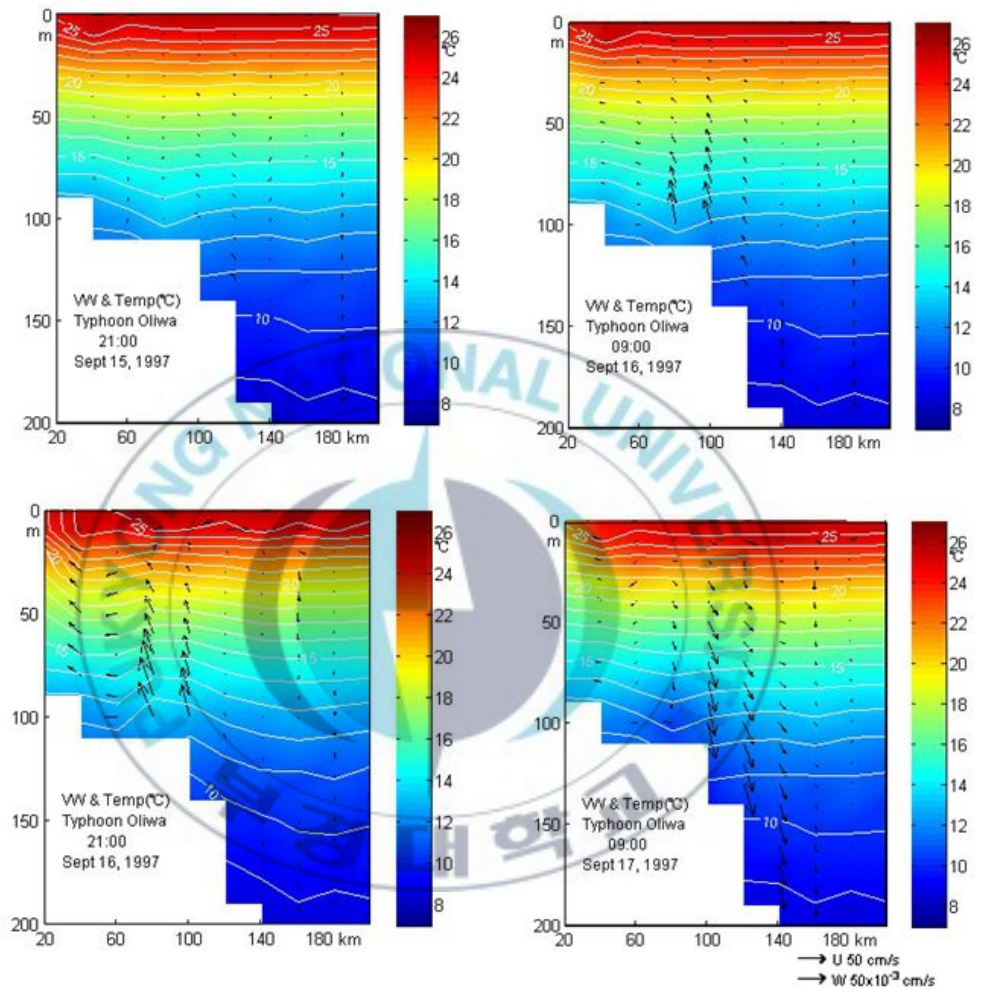
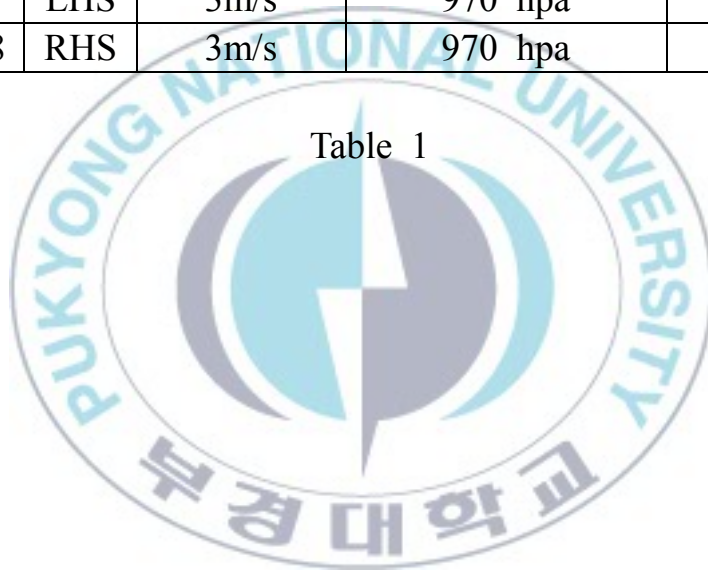


Figure 5

Condition	Track	Moving speed	Lowest central pressure	Grid interval
Case 1	CTR	3m/s	970 hpa	20km
Case 2	CTR	3m/s	950 hpa	20km
Case 3	CTR	3m/s	990 hpa	20km
Case 4	CTR	6m/s	970 hpa	20km
Case 5	CTR	9m/s	970 hpa	20km
Case 6	CTR	3m/s	970 hpa	10km
Case 7	LHS	3m/s	970 hpa	20km
Case 8	RHS	3m/s	970 hpa	20km

Table 1



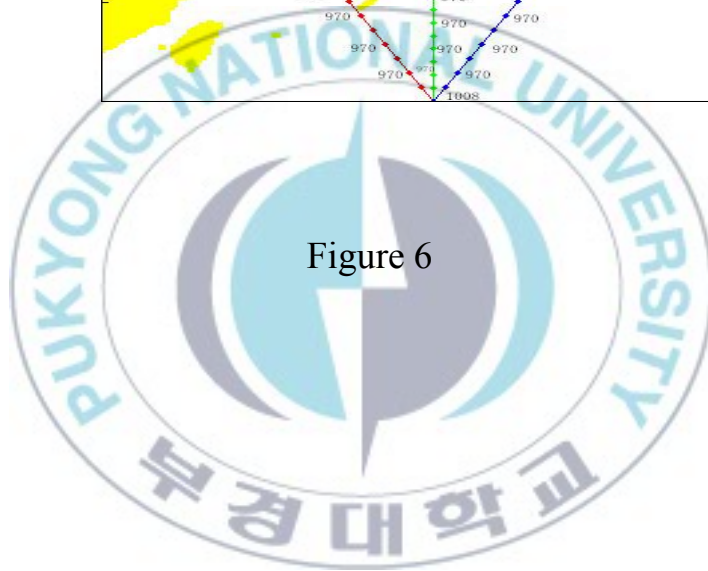
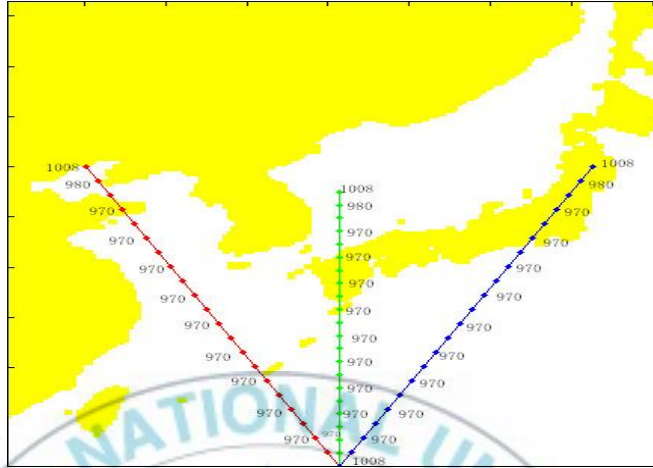


Figure 6

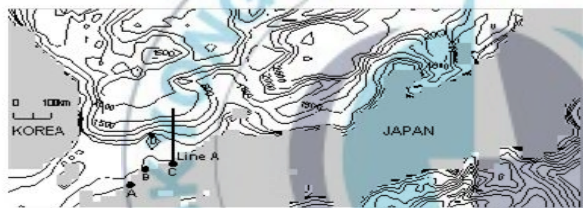
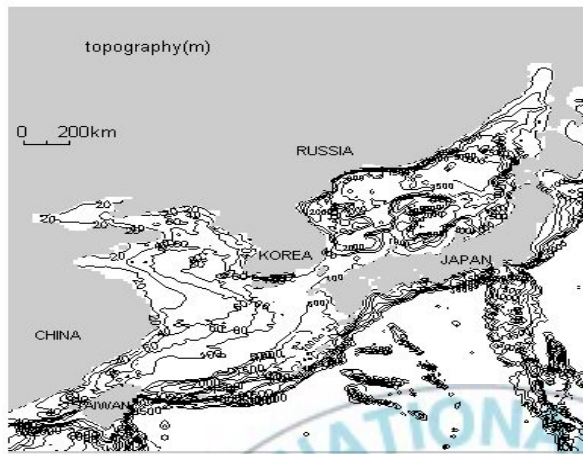


Figure 7

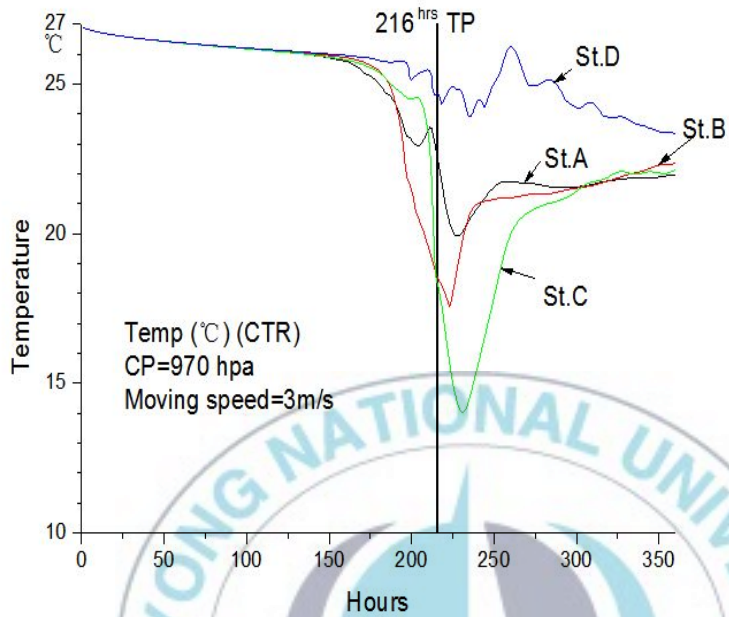


Figure 8

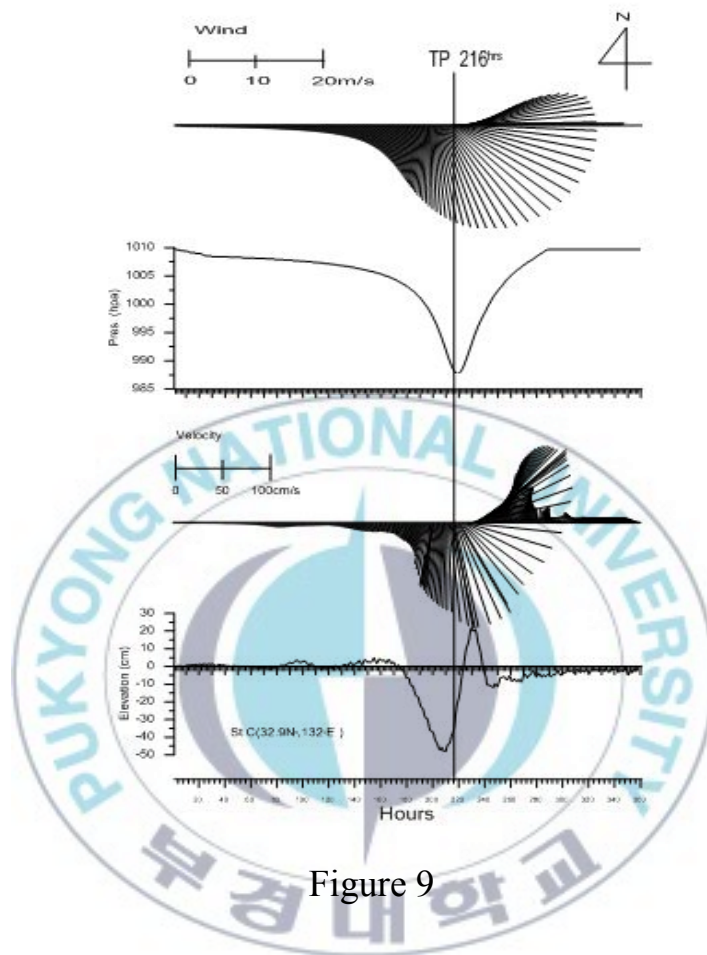


Figure 9

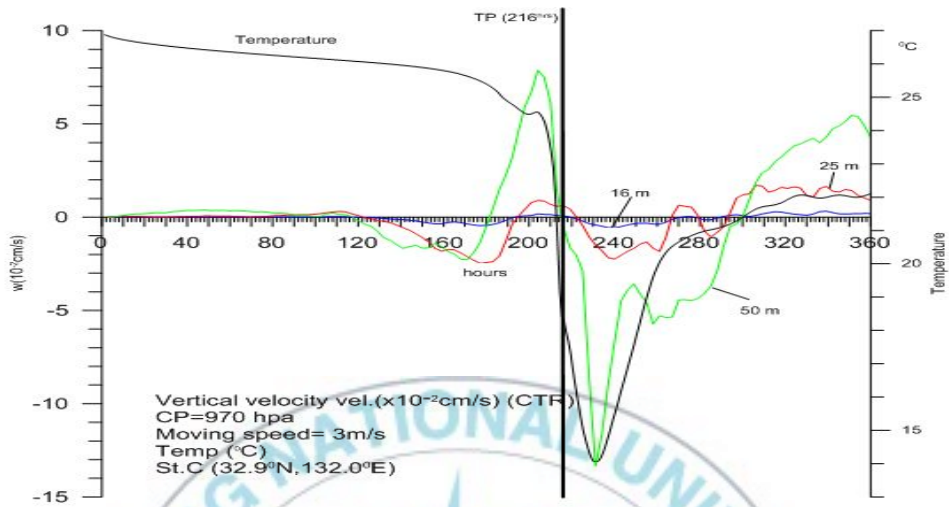
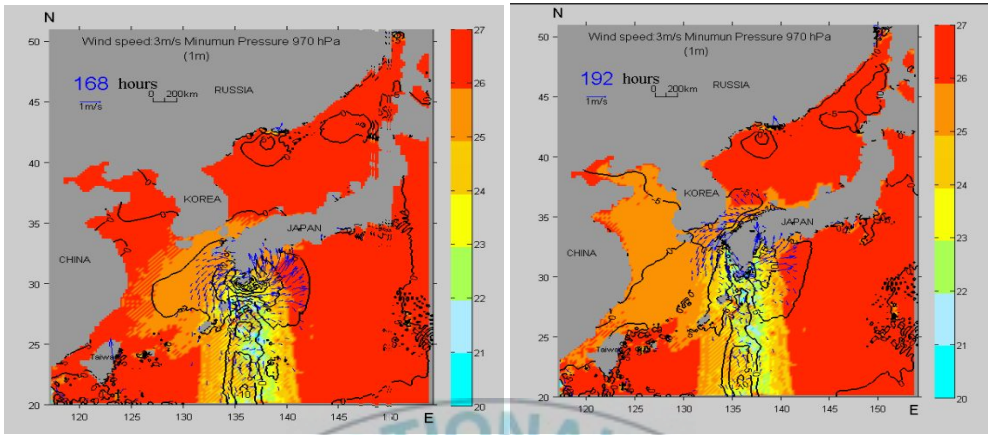
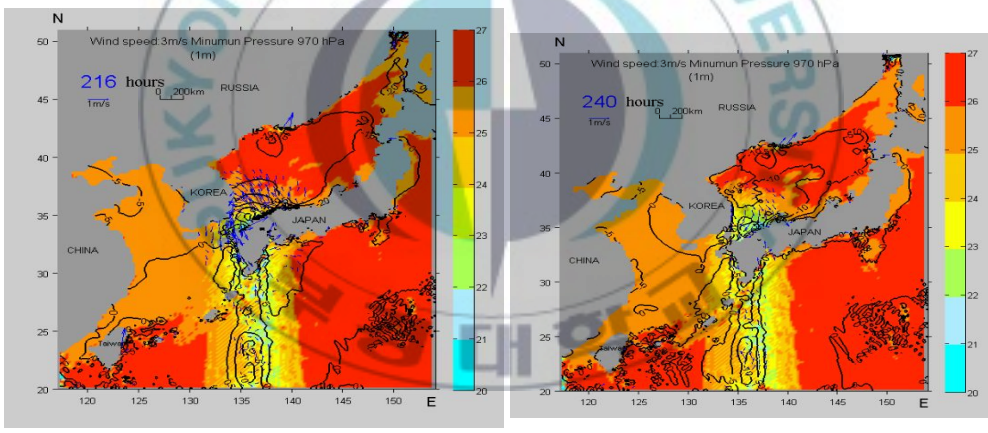


Figure 10



(a)

(b)



(c)

(d)

Figure 11

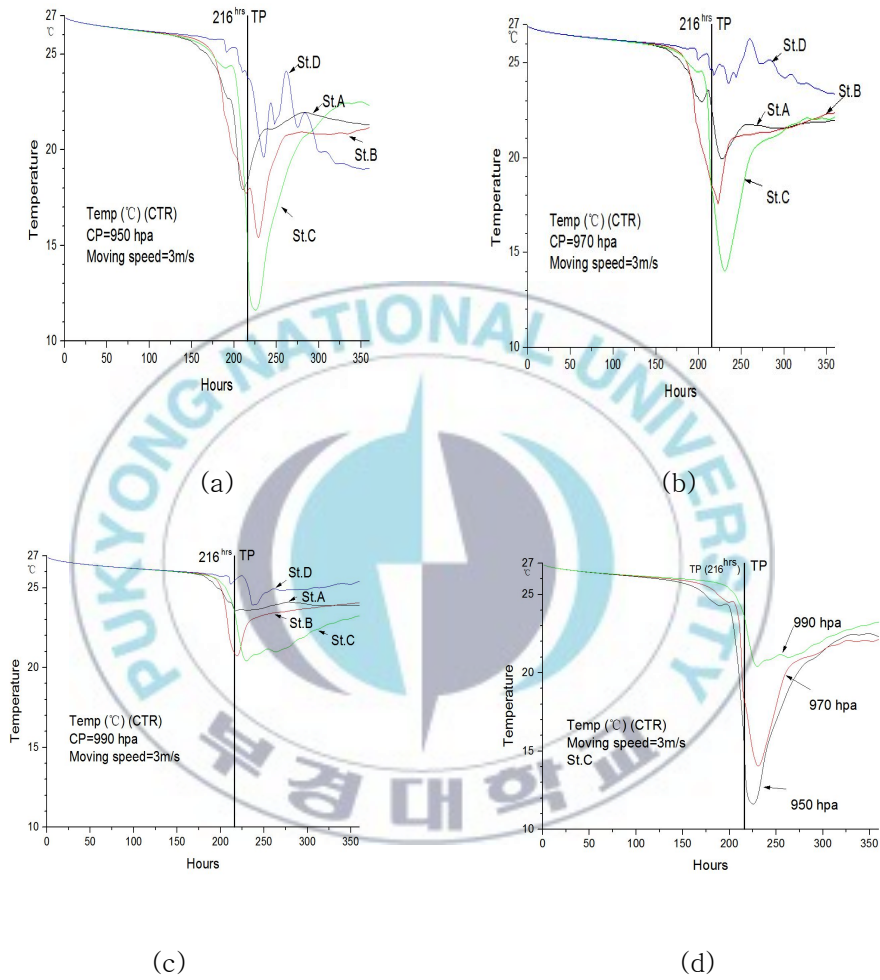


Figure 12

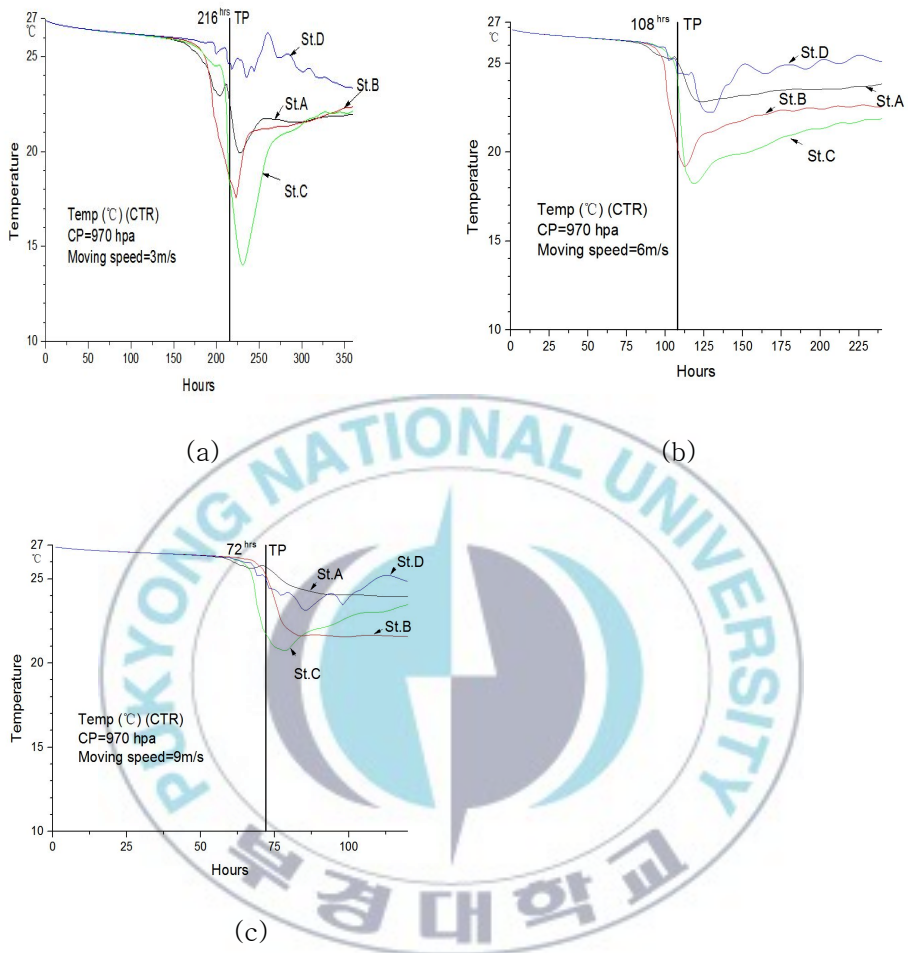
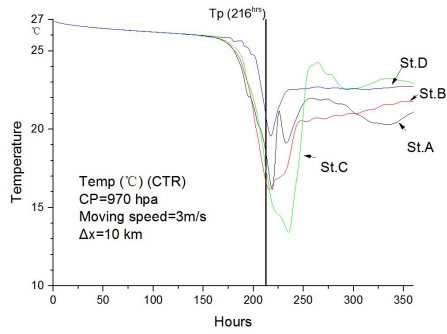
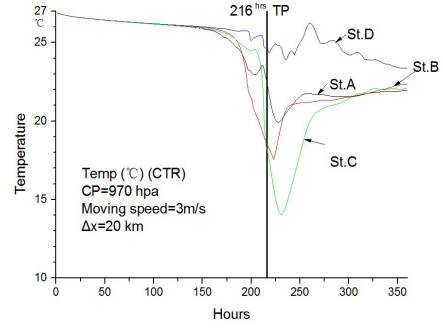


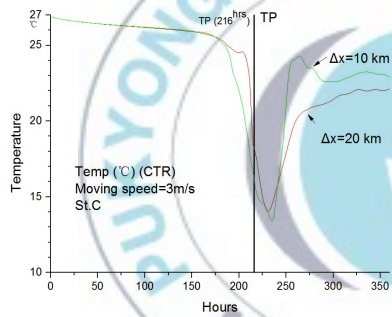
Figure 13



(a)

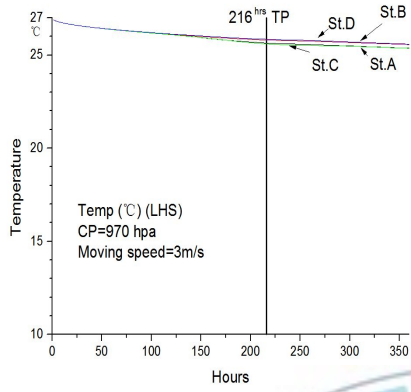


(b)

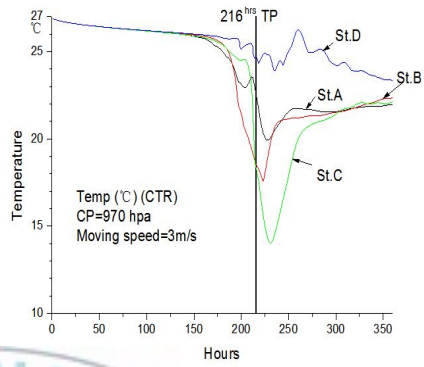


(c)

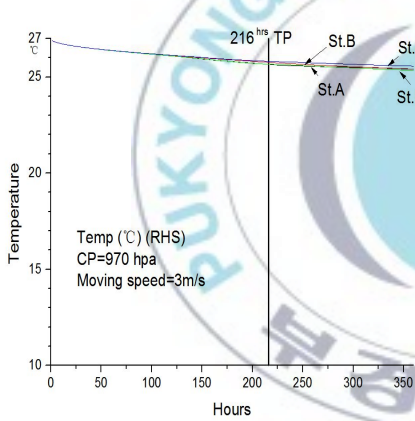
Figure 14



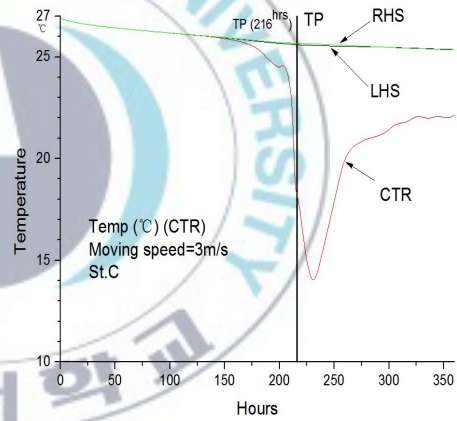
(a)



(b)



(c)



(d)

Figure 15

References

- Blumberg, A.F., and G.L. Mellor, A description of a three-dimensional coastal ocean circulation model. In Three Dimensional Coastal Ocean Models, Coastal Estuarine Science, vol. 4, edited by N. S. Heaps, AGU, Washington, D. C., 208 pp, 1987.
- Chen et al., 2003
- Colling, 1989
- Cushman-Roisin, B., Introduction to geophysical fluid dynamics. Prentice Hall, Englewood Cliffs, New Jersey, 320pp, 1994.
- Dongxiao Wang et al., Coastal upwelling in summer 2000 in the northeastern South China Sea, 2012
- Fujita, T., Pressure distribution within typhoon. *Geophys. Mag.*, 23, 437-451, 1952.
- Gill, A. E., Atmosphere-ocean dynamics. Academic press, New York, 666pp., 1982.
- Heaps, N.S., Storm surge, 1967-1982. *Geophys. J. Roy. Astron. Soc.*, 74, 331-367, 1983.
- Hong, C. H., and J. H. Yoon, A three-dimensional numerical simulation of Typhoon Holly in the northern Pacific Ocean. *J. Geophys. Res.*, 108(C8), 3282, doi:10.1029/2002JC001563, 2003
- Konishi T., and Y. Tsuji, Analysis of storm surges in the western part of the Seto inland sea of Japan caused by Typhoon 9119. *Continental Shelf Res.*, 15, 1795-1823, 1995.
- Lee et al, The Interaction of Supertyphoon Maemi (2003) with a

- Warm Ocean Eddy, 2003.s
- Lin et al, Response of sea surface temperature to chlorophyll-a concentration in the tropical Pacific: Annual mean, seasonal cycle, and interannual variability, 2011.
- M. García-Reyes and J. Largier, Observations of increased wind-driven coastal upwelling off central California, 2010
- Miyazaki, M., T. Ueno, and S. Unoki, Theoretical investigation of typhoon surges along the Japanese coast. *Oceanogr. Mag.*, 13, 51-75, 1961.
- Oke and Middleton, Topographically induced upwelling off Eastern Australia, *Journal of Physical Oceanography*, 30 (2000).
- Sakaida F, H. Kawamura, and Y. Toba, Sea surface cooling caused by typhoons in the Tohoku area in August 1989. *J. Geophys. Res.* 103, No. C1, 1053-1065, 1998
- Senju T, and T. Watanabe, A sudden temperature decrease along the San'in Coast induced by a typhoon. *UmutoSora*, 75, 1-8, 1999. (in Japanese with English abstract)
- Shoude Guan et al., Observed upper ocean response to typhoon Megi (2010) in the Northern South China Sea, 2014
- Siswanto et al., 2008;
- Suginohara, N., Onset of coastal upwelling in a two-layer ocean by wind stress with longshore variation. *J. Oceanogr. Soc. Japan*, 30, 23-33, 1974.
- Unoki S. I., I. Isozake, and S. Otsuka, Simulation of storm surges in Tokyo Bay, *Report of 2nd District Port Construction Bureau*, 125pp., 1964. (in Japanese with English abstract)

- Wada A., The processes of SST cooling by typhoon passage and case study of typhoon Rex with a mixed layer ocean model. *Meteorol. Geophys.*, 52, 31-66, 2002.
- Yoshida, K., Coastal upwelling off the California coast. *Rec. Oceanogr. Works Japan*. 2(2): 1-13, 1955.

